Turk J Phys
36 (2012) , 398 – 414.

doi:10.3906/fiz-1202-9

Full polar optical phonon states and dispersive spectra of a wurtzite GaN/AlN rectangular quantum wire

Li ZHANG
Institute of Electronic Technique and Material Development and
Department of Mechanism and Electronics, Guangzhou Panyu Polytechnic
Panyu 511483, People's Republic of CHINA
e-mail: zhangli-gz@263.net

Received: 08.02.2012

Abstract

Within the framework of the dielectric continuum model and Loudon's uniaxial crystal model, the full polar optical phonon modes including the quasi-confined (QC) modes, the propagating (PR) modes, the half-space (HS) modes, and the interface optical (IO) modes in a quasi-one-dimensional (Q1D) wurtzite rectangular quantum wire (QWR) structure are deduced and analyzed. The analytical phonon states, their dispersion equations and polar polarization eigenvectors are derived. Numerical calculation of dispersive spectra for these modes is performed on a wurtzite GaN/AlN rectangular QWR. The behavior of the QC mode reducing to the IO mode is observed clearly in the dispersive curves of these modes, which reveals that the present theories of phonon modes are self-consistency and correct for the description of phonon modes in wurtzite Q1D rectangular NW. These observations and results reveal that the confined dimensionality and cross-section shape influence greatly the dispersive properties of phonon modes in wurtzite quantum confined systems.

Key Words: Phonon modes, wurtzite heterostructure, rectangular quantum wires

Pacs: 78.67.Uh; 63.20.D-; 63.22.Gh; 81.05.Ea

1. Introduction

Currently, group III GaN-based semiconductor (including GaN, AlN, InN and their ternary compounds) quantum wires (QWRs) have attracted considerable amount of attention both in theoretical and experimental investigations [1–5]. The enormous deriving force behind these research efforts is mainly due to the three evident facts: the excellent properties of nitride materials, i.e. wide direct-band gap, large breakdown field, high carrier mobility and high thermal stability make the materials ideally suited for short-wavelength optoelectronic devices such as light emitting diodes and laser diodes, as well as for high-power and high-temperature electronics [6–9]; quasi-1-dimensional (Q1D) structure confinement of QWRs for carriers in two dimensions and freedom in the last dimension, promises more efficient lasers and optical gain as well as possible applications for optical

waveguide and photovoltaic elements in comparisons with quantum wells (QWs) and quantum dots (QDs) [10]; the Q1D QWR systems also play an important role in testing and understanding fundamental concepts, such as the role of dimensionality and size in optical, electrical and mechanical properties [4]. Hence the exploratory and research of electronic and optoelectronic properties in GaN-based QWRs has become a subject of interest for their concomitant advantages of possessing both excellent optoelectronic properties and nanoscale dimensions since the first GaN QWR was successfully synthesized [5].

Among the various investigations of physical properties in Q1D GaN based QWR structures, the dynamic features of crystal-lattice vibration have invoked researchers' special interest because of the importance of the crystal-lattice vibration for the design and work of quantum components and devices [11–13]. Quantum of crystal-lattice vibration, also known as the phonon, is one type of important elementary excitation in solid. In polar crystals, the polar optical phonons influence greatly not only the transport of carriers, but also the optic and optoelectronic properties, such as electron-phonon scattering, hot-electron relaxation, interband transition, and exciton lifetime, among other properties [14–18]. However, to the best of our knowledge, the polar optical phonon modes and dispersive spectra as well as corresponding electron-phonon interactions in Q1D GaN-based QWR structures have not been fully studied and understood [11, 12].

In general, the physical properties in the domain of nano-materials are expected to have close correlation with the cross section as well as their size and morphology [19, 20]. To understand how these factors influence their properties and to explore materials with potential applications, it is technically important to fabricate nano-materials with controllable geometries and analyze their various features in theories [21]. Based on the advanced MBE and MOCVD techniques, the Q1D GaN-based QWRs with cylindrical [10], hexagonal pyramid [22, 23], triangle [24, 25] and rectangular [26] cross-sections are fabricated in experiments, which depends on the growth-condition and material nature. Both theories and experiments reveal that, not only the electronic and optical properties, but also the crystal-lattice dynamics and dispersive spectra are affected greatly by the shape and size of cross-sections [27–29]. Though some phonon modes and their corresponding electron-phonon interactions in GaN cylindrical QWRs have been studied [11, 12, 30], the full polar optical phonon modes and their dispersive spectra in Q1D GaN-based QWRs with rectangular cross-section have not been investigated and fully understood. Hence it is necessary and important to investigate the crystal-lattice dynamic in wurtzite GaN-based rectangular QWR structures.

It is well known that nitrides usually crystallize in hexagonal wurtzite structure, whose physical properties exhibit anisotropy in space. Due to the decrease of the dimensionality (in contrast to 3-dimensionality bulk materials and the Q2D QWs), the properties of phonon modes in Q1D wurtzite QWRs may reveal many distinct new features. In fact, based on the dielectric continuum model (DCM), the polar vibrating properties of Q1D QWRs have been widely reported [27, 31–34]. For example, Stroscio [31] investigated the polar longitudinal-optical phonon modes in a Q1D rectangular quantum wire. After the work, the author and coworkers [32] also studied the surface optical phonon modes in a freestanding rectangular quantum wire. Later, Kim et al. [33] extended the work of surface phonon modes in freestanding Q1D GaAs quantum wires to that in Q1D GaAs/AlAs quantum wires. For cylindrical quantum wires, Xie et al. [27] have studied the surface optical (SO) and interface optical (IO) phonon modes in cylindrical quantum wires with infinite and finite potential boundary conditions (BCs). Zhang and Xie [34] solved the electrostatic potentials of IO modes in a multi-layer coupling cylindrical quantum wire by using transfer matrix method. All of the aforementioned works [27, 31–34] dealt with the optical phonon modes in cubic Q1D quantum systems. Within the framework of DCM and Loudon's

uniaxial crystal model [35], these works have been successfully extended from cubic quantum confined systems to wurtzite quantum wells [36, 37, 38] and wires [11]. For instance, Shi [36] solved exactly the equation of motion for the p-polarization field in an arbitrary wurtzite coupling QWs by employing the transfer matrix method. Lee et al. [37] studied the confined optical phonon modes and their scattering in wurtzite crystals and single and double planar heterostructures.

More recently, we investigated the IO phonon modes in a wurtzite GaN-AlN Q1D QWR with cylindrical crossing-section [11]. Apart from the common IO/SO phonon modes, the half-space (HS) mode and the confined phonon mode, some new phonon modes including the quasi-confined (QC) mode and the propagating (PR) mode are confirmed in the Q1D wurtzite nitride QWR heterostructures. Furthermore, part of these phonon modes (i.e. IO phonon modes) in Q2D wurtzite InN thin films and Q1D wurtzite GaN QWRs/nanorods have been observed and identified in the recent Raman scattering experiments [39] and time-resolved second-harmonic generation experiment [40].

Motivated by the phonon mode works of cubic Q1D QWR structure with rectangular cross-section mentioned above [31, 32, 33], we investigate the full polar optical phonon modes (including the IO, HS, QC and PR modes) in wurtzite rectangular quantum wires. Our motivation in part follows from two important facts: that geometric structures of the Q1D QWRs can greatly influence the optical phonon modes [28, 29], and that the anisotropy of wurtzite materials may result in more complicated optical phonon properties [11, 30, 36–38]. Up to now, aside from partial work into IO phonon modes [41], no investigation has fully studied polar optical phonon modes in Q1D wurtzite rectangular quantum wire systems. The intent of the present work is to fill a gap in optical phonon mode theories with respect to wurtzite rectangular QWRs. We study the fully phonon vibration modes and their dispersive spectra in a Q1D rectangular QWR structures in the present paper.

The paper is so organized: in Section 2, the polar phonon dispersion relations and electron-phonon coupling functions for the four types phonon modes, i.e. the QC, PR, HS and IO modes are deduced; in Section 3, the numerical results for the dispersion behavior of these modes in a chosen GaN/AlN QWR are carried out and discussed, and finally, the main results obtained in the current work are summarized in Section 4.

2. Theory

Let us consider a wurtzite GaN QWR with rectangular crossing-section embedded in GaAlN dielectric matrix (referring to Figure 1). We assume that the c-axis of the crystal is along the z-direction, and the widths of the QWR in x-and y-directions are $2\,L_x$ and $2\,L_y$, respectively. Within the macroscopic DCM, the vibration properties of a given Q1D QWR structure with free charge density $\rho(r) = 0$ are determined from the second-order differential equation [11, 12, 36]:

$$-\varepsilon_t(\omega)\nabla_t^2\Phi(\vec{r}\,) - \varepsilon_z(\omega)\nabla_z^2\Phi(\vec{r}\,) = 0 \tag{1}$$

where $\Phi(\vec{r}\,)$ is the scalar electrostatic potential of phonon modes, and $\varepsilon_t(\omega)$ and $\varepsilon_z(\omega)$ are the dielectric constants of the respective materials in t and $z$directions. The dielectric functions in two different directions are given by

$$\varepsilon_v(\omega) = \varepsilon_v^{\infty}\frac{\omega^2 - \omega_{v,L}^2}{\omega^2 - \omega_{v,T}^2}, \tag{2}$$

where $v = \{t,\ z\}$ denotes t- and z-directions, ε_v^{∞} is the high-frequency dielectric constant, and $\omega_{z,L}$, $\omega_{z,T}$, $\omega_{t,L}$ and $\omega_{t,T}$ are the zone center characteristic frequencies of A_1 (LO), A_1 (TO), E_1 (LO), and E_1 (TO) modes, respectively.

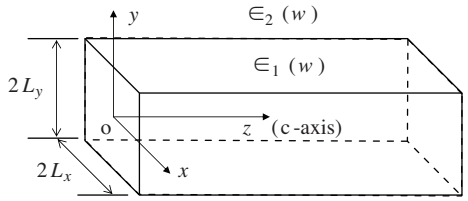

Figure 1. Schematic view of the wurtzite GaN/AlGaN rectangular QWR. The z-direction is taken along the c-axis of the wurtzite crystal materials.

Since this system is translationally invariant in the z-direction the electrostatic potential describing the optical-phonon modes may be taken as [31–33]

$$\Phi(\vec{r}\,) = \sum_{k_z} \varphi(x,y) e^{ik_z z}, \tag{3}$$

where k_z is the phonon wave-number in the z-direction. Finally, we get the equation in the right angle axes, i.e.

$$\left[\varepsilon_t(\omega)\left(\frac{\partial^2}{\partial x^2} + \frac{\partial^2}{\partial y^2}\right) - \varepsilon_z(\omega) k_z^2\right] \varphi(x,y) = 0, \tag{4}$$

Assuming the x- and y- dependent potentials are separable and requiring that $\varepsilon_t(\omega) \neq 0$ for dispersive phonon modes, it follows that

$$\frac{1}{\varphi_x(x)}\frac{d^2\varphi_x(x)}{dx^2} + \frac{1}{\varphi_y(y)}\frac{d^2\varphi_y(y)}{dy^2} - \xi_i(\omega)\gamma_i^2(\omega)k_z^2 = 0, \tag{5}$$

or

$$\alpha_i^2 + \beta_i^2 - \xi_i(\omega)\gamma_i^2(\omega)k_z^2 = 0 \quad (i = 1,2), \tag{6}$$

with

$$\begin{cases} \xi_i(\omega) = sign[\varepsilon_{zi}(\omega)\varepsilon_{ti}(\omega)] \\ \gamma_i(\omega) = \sqrt{|\varepsilon_{zi}(\omega)/\varepsilon_{ti}(\omega)|}. \end{cases} \tag{7}$$

The subscripts $i = 1, 2$ in equations (5)–(7) denote the GaN well and AlGaN barrier materials, respectively.

2.1. QC phonon modes

Due to the anisotropy of the wurtzite material the QC phonon modes may appear in the Q1D GaN/AlGaN QWRs which cannot exist in isotopic cubic GaAs-based quantum structures in general [36–38]. The QC phonon mode is one type of mode that behaves as vibrating waves in the well-layer material and as decaying waves in the barrier-layer dielectric material, whose characteristic is quite analogous to the bound electric states in finite-deep quantum confined systems [30]. In terms of this feature, equation (4) confirms that the function $\xi_1(\omega)$ should take negative values, and $\xi_2(\omega)$ should be positive values.

Let us analyze the phonon potentials of the QC modes in x-direction. The potential functions of QC modes in the QWRs are given by

$$\varphi^{S}_{QC}(x) = \begin{cases} C\exp(-\alpha_2|x|) & |x| > L_x, \\ C\cos(\alpha_1 x)\exp(-\alpha_2 L_x)/\cos(\alpha_1 L_x) & |x| \le L_x \end{cases} \tag{8}$$

and

$$\varphi^{A}_{QC}(x) = \begin{cases} C\,sign(x)\exp(-\alpha_2|x|) & |x| > L_x, \\ C\,\sin(\alpha_1 x)\exp(-\alpha_2 L_x)/\sin(\alpha_1 L_x) & |x| \le L_x. \end{cases} \tag{9}$$

Equations (8) and (9) correspond, respectively, to the symmetrical and antisymmetrical potential functions of QC modes in the QWR systems. The continuity of potential functions at $x = \pm L_x$ result in the relation

$$\begin{cases} \varepsilon_{t1}(\omega)\alpha_1\tan(\alpha_1 L_x) - \varepsilon_{t2}(\omega)\alpha_2 = 0 & (S), \\ \varepsilon_{t1}(\omega)\alpha_1\cot(\alpha_1 L_x) - \varepsilon_{t2}(\omega)\alpha_2 = 0 & (AS). \end{cases} \tag{10}$$

In the same way, by substituting α and L_x in equations (9) with β and L_y, respectively, one obtains the y-component of phonon potential functions for QC modes in the structures. Using the continuous conditions at the interfaces $y = \pm L_y$, the following relationships are obtained:

$$\begin{cases} \varepsilon_{t1}(\omega)\beta_1\tan(\beta_1 L_x) - \varepsilon_{t2}(\omega)\beta_2 = 0 & (S), \\ \varepsilon_{t1}(\omega)\beta_1\cot(\beta_1 L_x) - \varepsilon_{t2}(\omega)\beta_2 = 0 & (AS). \end{cases} \tag{11}$$

In fact, relationships (10) and (11) are just the dispersive equations of QC modes in rectangular wurtzite QWRs.

For solutions of $\varphi_{QC}(x)$ and $\phi_{QC}(y)$, where both are both either symmetric or antisymmetric [32, 33], it follows that

$$\alpha_i L_x = \beta_i L_y, \quad i = 1, 2. \tag{12}$$

Thus equations (6) and (12) require that

$$\alpha_i = \frac{\gamma_i k_z}{\sqrt{1 + (L_x/L_y)^2}}, \quad \beta_i = \frac{\gamma_i k_z}{\sqrt{1 + (L_y/L_x)^2}}, \quad i = 1, 2. \tag{13}$$

As discussed in references [31–33], where $\varphi_{QC}(x)$ and $\varphi_{QC}(y)$ have opposite parities, there will be no solutions satisfying simultaneously dispersion equations (10) and (11). Thus only the solutions where $\varphi_{QC}(x)$ and $\varphi_{QC}(y)$ have the same parities are permitted in Q1D QWR structures. The polarization eigenvectors for the symmetric and antisymmetric QC modes are given as follows:

$$\begin{aligned} P^{SS}_{QC,k_z}(\vec{r}) &= \tfrac{1-\varepsilon}{4\pi}\nabla\Phi^{SS}_{QC}(\vec{r}) = \tfrac{1-\varepsilon}{4\pi}\nabla\left[\Phi^{S}_{QC}(x)\Phi^{S}_{QC}(y)e^{ik_z z}\right] \\ &= \begin{cases} \frac{C^2\exp(-\alpha_2 L_x - \beta_2 L_y + ik_z z)}{4\pi\cos(\alpha_1 L_x)\cos(\beta_1 L_y)}[-\hat{x}\alpha_1(1-\varepsilon_{t1})\sin(\alpha_1 x) \\ \times\cos(\beta_1 y) - \hat{y}\beta_1(1-\varepsilon_{t1})\sin(\beta_1 y)\cos(\alpha_1 x) & In \\ +ik_z(1-\varepsilon_{z1})\cos(\alpha_1 x)\cos(\beta_1 y)\hat{z}], \\ \frac{C^2\exp(-\beta_2|y| - \alpha_2|x| + ik_z z)}{4\pi}[-\alpha_2(1-\varepsilon_{t2})\hat{x} \\ -\beta_2(1-\varepsilon_{t2})\hat{y} + ik_z(1-\varepsilon_{z1})\hat{z}] & Out \end{cases} \end{aligned} \tag{14}$$

and

$$P^{AA}_{QC,k_z}(\vec{r}) = \frac{1-\varepsilon}{4\pi}\nabla\Phi^{AA}_{QC}(\vec{r}) = \frac{1-\varepsilon}{4\pi}\nabla\left[\Phi^{A}_{QC}(x)\Phi A^{S}_{QC}(y)e^{ik_z z}\right]$$
$$= \begin{cases} \frac{C^2\exp(-\alpha_2 L_x-\beta_2 L_y+ik_z z)}{4\pi\sin(\alpha_1 L_x)\sin(\beta_1 L_y)}[\hat{x}\alpha_1(1-\varepsilon_{t1})\cos(\alpha_1 x) & \\ \times\sin(\beta_1 y)+\hat{y}\beta_1(1-\varepsilon_{t1})\cos(\beta_1 y)\sin(\alpha_1 x) & In \\ +ik_z(1-\varepsilon_{z1})\sin(\alpha_1 x)\sin(\beta_1 y)\hat{z}], & \\ \frac{C^2\exp(-\beta_2|y|-\alpha_2|x|+ik_z z)}{4\pi}[-\alpha_2(1-\varepsilon_{t2})\hat{x} & \\ -\beta_2(1-\varepsilon_{t2})\hat{y}+ik_z(1-\varepsilon_{z1})\hat{z}]. & Out \end{cases} \tag{15}$$

The labels "In" and "Out" denote those terms that are within and outside of the QWR ranges, respectively.

2.2. PR phonon modes

In isotropic cubic semiconductor materials such as GaAs-based quantum structures, there are no PR modes. The typical feature of PR modes is that they behave as vibrating waves in both well- and barrier-materials [42]. Based on this feature, the potential functions $\phi(x,y)$ should take the forms of vibrating waves. In terms of theories of second-order differential equation, this demands that the conditions $\xi_i(\omega) < 0$ (i =1, 2) [i.e., equation (7)] are satisfied. Taking into account the symmetry of the QWR structures, we obtained a symmetric solution of the form in x-direction for the PR modes as

$$\varphi^{S}_{PR}(x) = \begin{cases} C\cos(\alpha_2|x|) & |x| > L_x \\ C\cos(\alpha_1 x)\cos(\alpha_2 L_x)/\cos(\alpha_1 L_x) & |x| \le L_x, \end{cases} \tag{16}$$

and an antisymmetrical one as

$$\varphi^{A}_{PR}(x) = \begin{cases} C\sin(\alpha_2|x|) & |x| > L_x, \\ C\sin(\alpha_1 x)\sin(\alpha_2 L_x)/\sin(\alpha_1 L_x) & |x| \le L_x. \end{cases} \tag{17}$$

By further requiring that the x-components of electric displacement at the quantum wire boundaries, it is necessary that

$$\begin{cases} \varepsilon_{t1}(\omega)\alpha_1\tan(\alpha_1 L_x) - \varepsilon_{t2}(\omega)\alpha_2\tan(\alpha_2 L_x) = 0 & (S), \\ \varepsilon_{t1}(\omega)\alpha_1\cot(\alpha_1 L_x) - \varepsilon_{t2}(\omega)\alpha_2\cot(\alpha_1 L_x) = 0 & (AS). \end{cases} \tag{18}$$

Similar analysis finds that $\varphi_{PR}(y)$ should satisfy equations in the form of equations (16) and (17) where α, L_x and x are replaced by β, L_y and y, respectively. The continuity of y-components of electric displacement for the PR modes at the quantum wire boundaries hence implies

$$\begin{cases} \varepsilon_{t1}(\omega)\beta_1\tan(\beta_1 L_y) - \varepsilon_{t2}(\omega)\beta_2\tan(\beta_2 L_y) = 0 & (S), \\ \varepsilon_{t1}(\omega)\beta_1\cot(\beta_1 L_y) - \varepsilon_{t2}(\omega)\beta_2\cot(\beta_1 L_y) = 0 & (AS). \end{cases} \tag{19}$$

The polarization eigenvectors for the symmetric and antisymmetric modes may be obtained by using the relations $P(\vec{r}\,) = (1-\varepsilon)\nabla\Phi(\vec{r}\,)/4\pi$ on equations (16) and (17). They are given by the relations

$$P^{SS}_{PR,k_z}(\vec{r}) = \tfrac{1-\varepsilon}{4\pi}\nabla\Phi^{SS}_{PR}(\vec{r}) = \tfrac{1-\varepsilon}{4\pi}\nabla\left[\Phi^{S}_{PR}(x)\Phi^{S}_{PR}(y)e^{ik_z z}\right]$$

$$= \begin{cases} \frac{C^2\cos(\alpha_2 L_x)\cos(\beta_2 L_y)\exp(ik_z z)}{4\pi\cos(\alpha_1 L_x)\cos(\beta_1 L_y)}[-\hat{x}\alpha_1(1-\varepsilon_{t1})\sin(\alpha_1 x) & \\ \times\cos(\beta_1 y) - \beta_1(1-\varepsilon_{t1})\sin(\beta_1 y)\cos(\alpha_1 x)\hat{y} & In \\ +ik_z(1-\varepsilon_{z1})\cos(\alpha_1 x)\cos(\beta_1 y)\hat{z}], & \\ \frac{C^2\exp(ik_z z)}{4\pi}[-\alpha_2(1-\varepsilon_{t2})\sin(\alpha_2 x)\cos(\beta_2 y)\hat{x} & \\ -\beta_2(1-\varepsilon_{t2})\sin(\beta_2 y)\cos(\alpha_2 x)\hat{y} & Out \\ +ik_z(1-\varepsilon_{z2})\cos(\beta_2 y)\cos(\alpha_2 x)\hat{z}], & \end{cases} \tag{20}$$

and

$$P^{AA}_{PR,k_z}(\vec{r}) = \tfrac{1-\varepsilon}{4\pi}\nabla\Phi^{AA}_{PR}(\vec{r}) = \tfrac{1-\varepsilon}{4\pi}\nabla\left[\Phi^{A}_{PR}(x)\Phi^{A}_{PR}(y)e^{ik_z z}\right]$$

$$= \begin{cases} \frac{C^2\sin(\alpha_2 L_x)\sin(\beta_2 L_y)\exp(ik_z z)}{4\pi\sin(\alpha_1 L_x)\sin(\beta_1 L_y)}[\hat{x}\alpha_1(1-\varepsilon_{t1})\cos(\alpha_1 x) & \\ \times\sin(\beta_1 y) - \beta_1(1-\varepsilon_{t1})\cos(\beta_1 y)\sin(\alpha_1 x)\hat{y} & In \\ +ik_z(1-\varepsilon_{z1})\sin(\alpha_1 x)\sin(\beta_1 y)\hat{z}], & \\ \frac{C^2\exp(ik_z z)}{4\pi}[-\alpha_2(1-\varepsilon_{t2})\cos(\alpha_2 x)\sin(\beta_2 y)\hat{x} & \\ +\beta_2(1-\varepsilon_{t2})\cos(\beta_2 y)\sin(\alpha_2 x)\hat{y} & Out \\ +ik_z(1-\varepsilon_{z2})\sin(\beta_2 y)\sin(\alpha_2 x)\hat{z}]. & \end{cases} \tag{21}$$

.

2.3. HS phonon modes

The HS phonon modes appear not only in cubic semiconductor quantum systems [43], but also in wurtzite quantum structures. The HS modes behave as decaying waves in well-layer materials, and as vibrating waves in barrier-layer materials, which is just opposite to the cases of the QC modes. Based on the characteristic, the functions $\xi_1(\omega)$ should be positive within the wurtzite QWR range, while $\xi_2(\omega)$ should be negative outside the QWR range (i.e., a dielectric environment). Thus the phonon potentials of the wurtzite rectangular QWRs in x-direction are written as

$$\varphi^{S}_{HS}(x) = \begin{cases} C\cos(\alpha_2 x) & |x| > L_x, \\ C\cosh(\alpha_1 x)\cos(\alpha_2 L_x)/\cosh(\alpha_1 L_x) & |x| \le L_x \end{cases} \tag{22}$$

for the symmetrical HS phonon modes and

$$\varphi^{A}_{HS}(x) = \begin{cases} C\sin(\alpha_2 x) & |x| > L_x, \\ C\sinh(\alpha_1 x)\sin(\alpha_2 L_x)/\sinh(\alpha_1 L_x) & |x| \le L_x \end{cases} \tag{23}$$

for the antisymmetrical HS modes. Similarly, the HS phonon potentials in the y-direction can also be written by substituting α and L_x with β and L_y. Adding the continues condition at the rectangular QWR interfaces,

one gets

$$\begin{cases} \varepsilon_{t1}(\omega)\alpha_1 \tanh(\alpha_1 L_x) + \varepsilon_{t2}(\omega)\alpha_2 \tan(\alpha_2 L_x) = 0 & (S), \\ \varepsilon_{t1}(\omega)\alpha_1 \coth(\alpha_1 L_x) - \varepsilon_{t2}(\omega)\alpha_2 \cot(\alpha_1 L_x) = 0 & (AS), \end{cases} \tag{24}$$

and

$$\begin{cases} \varepsilon_{t1}(\omega)\beta_1 \tanh(\beta_1 L_y) + \varepsilon_{t2}(\omega)\beta_2 \tan(\beta_2 L_y) = 0 & (S), \\ \varepsilon_{t1}(\omega)\beta_1 \coth(\beta_1 L_y) - \varepsilon_{t2}(\omega)\beta_2 \cot(\beta_1 L_y) = 0 & (AS), \end{cases} \tag{25}$$

The polarization eigenvectors of HS modes in the wurtzite QWRs are given by

$$P^{SS}_{HS,k_z}(\vec{r}) = \tfrac{1-\varepsilon}{4\pi}\nabla\Phi^{SS}_{HS}(\vec{r}) = \tfrac{1-\varepsilon}{4\pi}\nabla\left[\Phi^{S}_{HS}(x)\Phi^{S}_{HS}(y)e^{ik_z z}\right]$$

$$= \begin{cases} \frac{C^2\cos(\alpha_2 L_x)\cos(\beta_2 L_y)\exp(ik_z z)}{4\pi\cosh(\alpha_1 L_x)\cosh(\beta_1 L_y)}[\hat{x}\alpha_1(1-\varepsilon_{t1})\sinh(\alpha_1 x) & \\ \times\cosh(\beta_1 y) + \beta_1(1-\varepsilon_{t1})\sinh(\beta_1 y)\cosh(\alpha_1 x)\hat{y} & In \\ +ik_z(1-\varepsilon_{z1})\cosh(\alpha_1 x)\cosh(\beta_1 y)\hat{z}], & \\ \frac{C^2\exp(ik_z z)}{4\pi}[-\alpha_2(1-\varepsilon_{t2})\sin(\alpha_2 x)\cos(\beta_2 y)\hat{x} & \\ -\beta_2(1-\varepsilon_{t2})\sin(\beta_2 y)\cos(\alpha_2 x)\hat{y} & Out \\ +ik_z(1-\varepsilon_{z2})\cos(\beta_2 y)\cos(\alpha_2 x)\hat{z}] & \end{cases} \tag{26}$$

for symmetrical HS phonon modes, and

$$P^{AA}_{HS,k_z}(\vec{r}) = \tfrac{1-\varepsilon}{4\pi}\nabla\Phi^{SS}_{HS}(\vec{r}) = \tfrac{1-\varepsilon}{4\pi}\nabla\left[\Phi^{A}_{HS}(x)\Phi^{A}_{HS}(y)e^{ik_z z}\right]$$

$$= \begin{cases} \frac{C^2\sin(\alpha_2 L_x)\sin(\beta_2 L_y)\exp(ik_z z)}{4\pi\sinh(\alpha_1 L_x)\sinh(\beta_1 L_y)}[\hat{x}\alpha_1(1-\varepsilon_{t1})\cosh(\alpha_1 x) & \\ \times\sinh(\beta_1 y) + \beta_1(1-\varepsilon_{t1})\cosh(\beta_1 y)\sinh(\alpha_1 x)\hat{y} & In \\ +ik_z(1-\varepsilon_{z1})\sinh(\alpha_1 x)\sinh(\beta_1 y)\hat{z}], & \\ \frac{C^2\exp(ik_z z)}{4\pi}[\alpha_2(1-\varepsilon_{t2})\cos(\alpha_2 x)\sin(\beta_2 y)\hat{x} & \\ +\beta_2(1-\varepsilon_{t2})\cos(\beta_2 y)\sin(\alpha_2 x)\hat{y} & Out \\ +ik_z(1-\varepsilon_{z2})\sin(\beta_2 y)\sin(\alpha_2 x)\hat{z}] & \end{cases} \tag{27}$$

for the antisymmetrical HS phonon modes.

2.4. IO phonon modes

The IO phonon mode is one modes whose electrostatic potential maximizes at the interfaces, and then decays on both sides of each interface. The IO phonon modes behave as decaying waves in all of the material layers. These features demand that the functions $\xi_i(\omega)$ (i =1, 2) take positive in the well and barrier materials. Thus IO phonon modes can exist in isotropic cubic semiconductor nanowires or in anisotropic wurtzite QWRs. We obtained a symmetric solution of the form in x-direction for the IO modes [41] in the form

$$\varphi^{S}_{IO}(x) = \begin{cases} C\exp(-\alpha_2|x|) & |x| > L_x, \\ C\cosh(\alpha_1 x)\exp(-\alpha_2 L_x)/\cosh(\alpha_1 L_x) & |x| \le L_x. \end{cases} \tag{28}$$

An antisymmetric solution is

$$\varphi^{A}_{IO}(x)=\begin{cases} C\ sign(x)\exp(-\alpha_2|x|) & |x|>L_x,\\ C\ \sinh(\alpha_1 x)\exp(-\alpha_2 L_x)/\sinh(\alpha_1 L_x) & |x|\le L_x. \end{cases} \tag{29}$$

The continuity of electric displacement in x-direction at the quantum wire boundaries implies

$$\begin{cases} \varepsilon_{t1}(\omega)\alpha_1\tanh(\alpha_1 L_x)+\varepsilon_{t2}(\omega)\alpha_2=0 & (S),\\ \varepsilon_{t1}(\omega)\alpha_1\coth(\alpha_1 L_x)+\varepsilon_{t2}(\omega)=0 & (AS). \end{cases} \tag{30}$$

The potential functions of IO phonon modes in the y-direction can be given similarly. Using these results with $P(\vec{r}\,)=(1-\varepsilon)\nabla\Phi(\vec{r}\,)/4\pi$, the polarization eigenvectors for the symmetric IO modes $P^{SS}_{k_z}(\vec{r}\,)$ and the antisymmetric IO modes $P^{AA}_{k_z}(\vec{r}\,)$ are obtained, i.e.,

$$\begin{aligned} P^{SS}_{IO,k_z}(\vec{r}) &= \tfrac{1-\varepsilon}{4\pi}\nabla\Phi^{SS}_{IO}(\vec{r})=\tfrac{1-\varepsilon}{4\pi}\nabla\left[\Phi^{S}_{IO}(x)\Phi^{S}_{IO}(y)e^{ik_z z}\right]\\ &=\begin{cases} \frac{C^2\exp(-\alpha_2 L_x-\beta_2 L_y+ik_z z)}{4\pi\cosh(\alpha_1 L_x)\cosh(\beta_1 L_y)}[\hat{x}\alpha_1(1-\varepsilon_{t1})\sinh(\alpha_1 x)\\ \times\cosh(\beta_1 y)+\beta_1(1-\varepsilon_{t1})\sinh(\beta_1 y)\cosh(\alpha_1 x)\hat{y} & In\\ +ik_z(1-\varepsilon_{z1})\cosh(\alpha_1 x)\cosh(\beta_1 y)\hat{z}],\\ \frac{C^2\exp(-\alpha_2|x|-\beta_2|y|+ik_z z)}{4\pi}[-\alpha_2(1-\varepsilon_{t2})\hat{x}\\ -\beta_2(1-\varepsilon_{t2})\hat{y}+ik_z(1-\varepsilon_{z2})\hat{z}], & Out \end{cases} \end{aligned} \tag{31}$$

and

$$\begin{aligned} P^{AA}_{IO,k_z}(\vec{r}) &= \tfrac{1-\varepsilon}{4\pi}\nabla\Phi^{AA}_{IO}(\vec{r})=\tfrac{1-\varepsilon}{4\pi}\nabla\left[\Phi^{A}_{IO}(x)\Phi^{A}_{IO}(y)e^{ik_z z}\right]\\ &=\begin{cases} \frac{C^2\exp(-\alpha_2 L_x-\beta_2 L_y+ik_z z)}{4\pi\cosh(\alpha_1 L_x)\cosh(\beta_1 L_y)}[\hat{x}\alpha_1(1-\varepsilon_{t1})\cosh(\alpha_1 x)\\ \times\sinh(\beta_1 y)+\beta_1(1-\varepsilon_{t1})\cosh(\beta_1 y)\sinh(\alpha_1 x)\hat{y} & In\\ +ik_z(1-\varepsilon_{z1})\sinh(\alpha_1 x)\sinh(\beta_1 y)\hat{z}],\\ \frac{C^2\exp(-\alpha_2|x|-\beta_2|y|+ik_z z)}{4\pi}[-\alpha_2(1-\varepsilon_{t2})\hat{x}\\ -\beta_2(1-\varepsilon_{t2})\hat{y}+ik_z(1-\varepsilon_{z2})\hat{z}]. & Out \end{cases} \end{aligned} \tag{32}$$

Once the anisotropy of wurtzite crystal materials are neglected (i.e. $\gamma_i\equiv 1$), the results of IO phonon modes obtained here can be naturally reduced to the cases in isotropy Q1D quantum wire systems [31–33], which reveals that the present results presented herein are more general than the previous ones reported.

3. Numerical results and discussion

In the present section, we discuss the dispersion spectra properties of the full optical phonon modes in a rectangular wurtzite GaN/AlN QWR system. The discussions are focus on the dependence of phonon modes dispersive frequencies on the free wave-vector k_z in z-directions. The sizes of the rectangular QWR are kept at $L_x=L_y=5$ nm. The material parameters used in our calculations are listed in Table 1 [36, 38].

Table 1. Zone-center energies (in meV) of polar optical phonons, and optical and static dielectric constant of wurtzite AlN and GaN [36, 38].

Material	A_1(TO)	E_1(TO)	A_1(LO)	E_1(LO)	ε^{∞}
GaN	67.89	73.22	92.08	94.06	5.35
AlN	75.72	83.13	110.30	113.02	4.77

It is necessary to discuss briefly the physical model of wurtzite GaN/AlN QWR with rectangular cross-section chosen here. In fact, the theoretical results of various phonon modes derived in the present work are applicable to all the wurtzite GaN/AlGaN and InGaN/GaN rectangular QWR systems if DCM is valid. Taking into account the situation that the Q1D binary GaN/AlN QWRs seem be easily fabricated in experiments [44–48] in contrast to ternary nitride QWR structures, only the GaN/AlN QWR structure is chosen on which to perform numerical analysis. On the other hand, the phonon spectra of Q2D planar GaN/AlN QWs [36–38, 42] and the Q1D cylindrical GaN/AlN QWRs [11] were widely reported. Thus the present discussions of dispersive phonon spectra on the rectangular GaN/AlN QWRs are convenient to compare with these previous results [11, 36–38, 42]. In additional, due to the fact that ternary $Al_xGa_{1-x}N$ and $In_xGa_{1x}N$ alloys usually present one-mode and two-mode behaviors for polar phonon modes [49–54], the phonon spectra in rectangular GaN/$Al_xGa_{1-x}N$ and $In_xGa_{1-x}N$/GaN QWR may be quite complicated. For simplicity, only the binary GaN/AlN rectangular QWRs are selected to analyze the dispersive properties of phonon modes here. Of course, we also have interest in the effects of ternary mixed crystals on the phonon spectra features of the wurtzite rectangular QWR structures; and we intend to report related work in this area in the near future.

Based on the parameters given in Table 1 and the above discussion on phonon mode types and characteristic, we find there are three types of polar phonon modes: the QC, IO and HS modes coexisting in the GaN/AlN QWR structures. Moreover, each phonon mode can appear in two frequency ranges. As discussed above, though the PR phonon modes may exist in GaN/AlGaN quantum structures, the PR phonon modes do not appear in the GaN/AlN QWRs. The PR phonon modes need both the negative function values of ξ_1 and ξ_2 for both well- and barrier-materials. But no frequency range which satisfies both negative ξ_i (i =1, 2) values exists in Table 2. Thus there is no PR phonon mode in the GaN/AlN QWR structures [11]. Detailed situations are displayed in Table 2. The symbol "$\sim$" in the table denotes the beginning value of the next and adjacent frequency range. And the superscripts "L" and "H" are used to distinguish these phonon modes in the low-and high-frequency ranges, respectively. It is noted that the range [ω_{tT2},ω_{zL1}] is forbidden because all the dispersive equations have no solution in this frequency range. This is a general feature of polar optical phonon modes in quantum confined systems [11, 12, 38, 43].

Table 2. Signs of the function $\xi i(\omega)(i$ =1, 2) and phonon mode types in seven frequency ranges divided by the characteristic frequencies of GaN and AlN materials.

Ranges	[$\omega_{zT1}\sim$]	[$\omega_{tT1}\sim$]	[$\omega_{zT2}\sim$]	[$\omega_{tT2}\sim$]	[$\omega_{zL1}\sim$]	[$\omega_{tL1}\sim$]	[$\omega_{zL2}\omega_{tL2}$]
$\xi_1(\omega)$	-	+	+	+	-	+	+
$\xi_2(\omega)$	+	+	-	+	+	+	-
Modes	QC^L	IO^L	HS^L	Forbidden	QC^H	IO^H	HS^H

The dispersive frequencies $\hbar\omega$ of HS phonon modes in low-frequency and high-frequency ranges as a function of phonon wave-number k_z in free z-direction are plotted in Figures 2 and 3, respectively. The solid

lines and dashed lines correspond respectively the symmetrical (HS_{Si}) and antisymmetric (HS_{Ai}) HS modes. From the figures, it is observed clearly that the dispersive spectra of HS modes in Figure 2 (Figure 3) are just within the low (hight-) frequency range of HS modes, i.e. $[\omega_{zT2},\omega_{tT2}]$ ($[\omega_{zL2},\omega_{tL2}]$), which are completely consistent with the observation in Table 2. There are infinite branches of HS phonon modes for a given k_z in the Q1D GaN/AlN rectangular QWR systems. Only the first four branches of HS modes are displayed for simplicity in each frequency range here. All the HS modes in low-frequency range ($HS^L_{A/S,i}$ modes in Figure 2) are the monotonic and increasing functions of wave-number k_z, while those in low-frequency range ($HS^H_{A/S,i}$ modes in Figure 3) are the monotonic and decreasing functions of wave-number k_z. As k_z approaches zero, the dispersive frequencies of all the $HS^L_{A/S,i}$ modes converge to the characteristic frequency ω_{zT2}, and those of all the $HS^H_{A/S,i}$ modes converge to the another characteristic frequency ω_{tT2} for AlN material. The dispersive frequencies of the antisymmetric $HS^L_{A,i}$ modes are always higher than those of the corresponding symmetrical $HS^L_{S,i}$ modes (Figure 2). This means that the antisymmetric $HS^L_{A,i}$ modes are more dispersive than the symmetrical ones. But for the $HS^H_{A/S,i}$ modes in high-frequency range (Figure 3), the case is just opposite, i.e the symmetrical $HS^H_{S,i}$ modes are more dispersive than the antisymmetrical ones. The HS phonon modes are not specific for wurtzite quantum confined systems, which also can appear in isotropic cubic quantum systems [36].

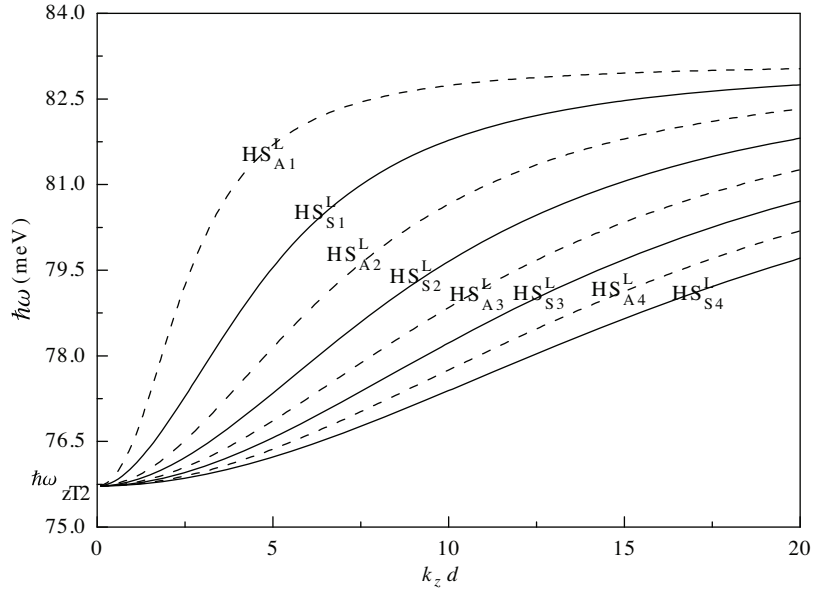

Figure 2. Dispersive frequencies $\hbar\omega$ of HS phonon modes in low-frequency range as a function of the phonon wave-number k_z in the Q1D wurtzite GaN/AlN rectangular QWR.

Figure 4 depicts the dispersive frequencies $\hbar\omega$ of the IO phonon modes in high-frequency range as a function of k_z. It is seen clearly that there are two branches of IO^H phonon modes: one branch of symmetrical modes IO^H_S (Solid line) and one branch of antisymmetrical modes IO^H_A (Dash line) in the QWR systems. The dispersion of each branch of IO^H mode is more obvious only when k_z is relatively small. These are the common behaviors of phonon modes in quantum confined structures, which are completely analogous to the cubic rectangular GaAa-based quantum wires [31–33]. When wave number $k_z \to \infty$, the

frequencies of the two branches of IO^H modes converge to a certain limited constant value 103.5 meV. Via detailed analysis, it is found that the limited frequency value 103.5 meV is just one solution of the equation $\sqrt{\varepsilon_{z1}(\omega)\varepsilon_{t1}(\omega)} - \sqrt{\varepsilon_{z2}(\omega)\varepsilon_{t2}(\omega)} = 0$. This equation determines the frequency of the IO phonons in single wurtzite planar GaN-based heterostructure [36]. In fact, as $k_z \to \infty$, the functions $\tanh(\alpha_1 L_x)\tanh(\beta_1 L_y)$, $\coth(\alpha_1 L_x)$ and $\coth(\beta_1 L_y)$ approach unity, the dispersion of IO modes in the Q1D rectangular QWRs can be reduced naturally to the identical form given above. The profound physical reason lie in the fact that IO modes cannot distinguish the planar and curved heterostructures due to large (small) enough free wave-number (wave-length) of IO phonon modes [55].

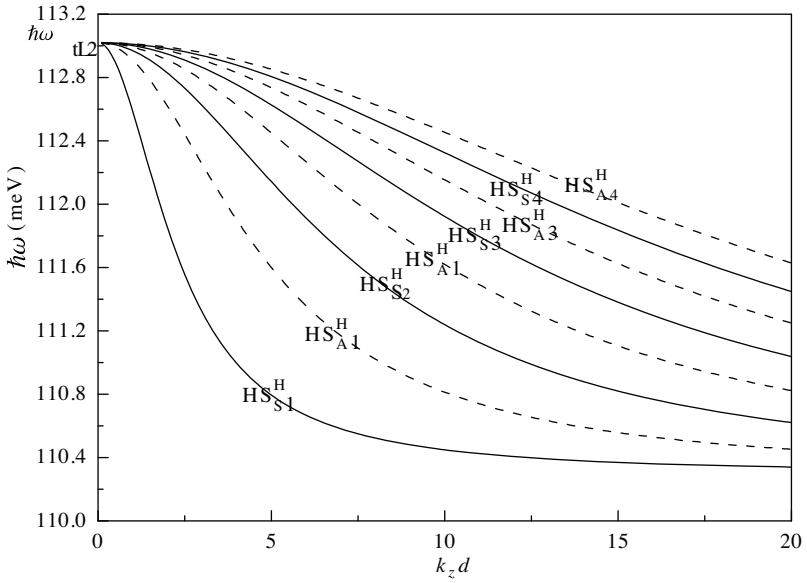

Figure 3. Dispersive frequencies $\hbar\omega$ of HS phonon modes in high-frequency range as a function of k_z in the wurtzite rectangular QWR.

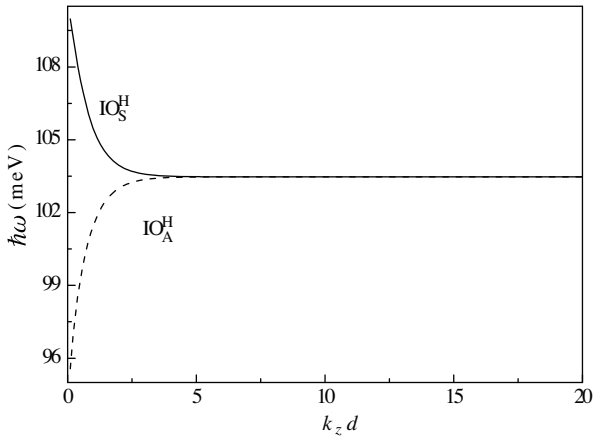

Figure 4. Dispersive frequencies $\hbar\omega$ of the IO phonon modes in high-frequency range as a function of k_z in the QWR structure.

The dispersive spectra of QC phonon modes in the high-frequency range as a function of the wave number k_z are shown in Figure 5. Only the first four branches of the symmetrical and antisymmetrical QC modes are given here. As k_z approaches zero, the frequencies of all the QC modes converge to the characteristic value of ω_{tL1} for GaN material. The other features of these dispersive curves for QC^H modes are quite similar to those for HS modes in high-frequency range (see Figure 3).

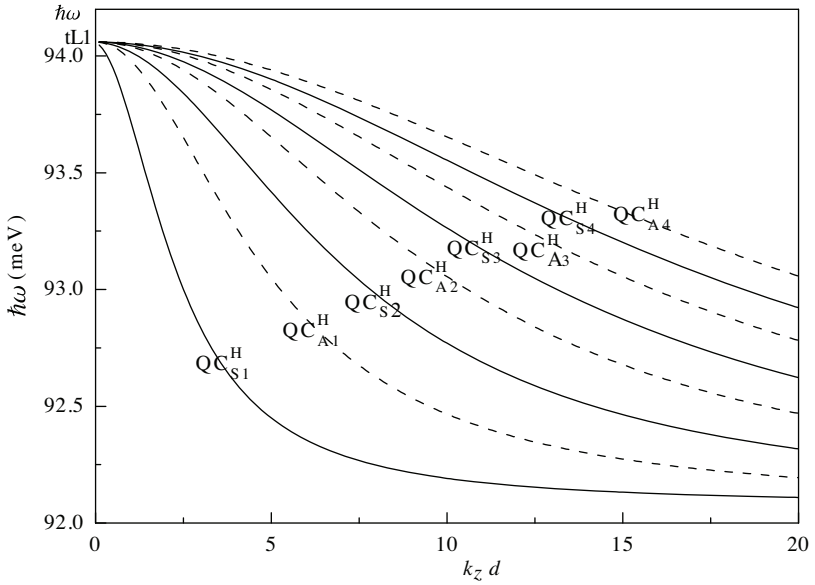

Figure 5. Dispersive spectra of QC phonon modes in high-frequency range as a function of the wave number k_z in the QWR system.

Figure 6 plots the dispersive spectra of QC modes and the IO modes in low-frequency range as a function of k_z in the GaN/AlN QWR system. The solid (dashed) curves correspond to the symmetrical (antisymmetrical) phonon modes. For a certain wave number k_z there are infinite branches of QC^L phonon modes, and only the first four branches of symmetrical and antisymmetrical modes are considered for simplicity here. But only one or two branches of IO^L modes exist in the Q1D GaN/AlN QWRs for a given k_z. As $k_z d < 3$, only one branch of antisymmetrical IO_A^L appear. And both the symmetrical and antisymmetrical $IO_{A/S}^L$ appear when the wave-number $k_z d$ is over than 3. As k_z approaches infinity, the frequencies of both $IO_{A/S}^L$ converge to 73.98 meV. The related mathematical and physical reasons for this observation are analyzed deeply above in Figure 4. It is interesting to note that the symmetrical QC_{S1}^L mode will reduce to the symmetrical IO_S^L phonon modes as its frequency is over than the characteristic frequency ω_{tT1} This is the typical reducing behavior of different types of phonon modes in wurtzite quantum systems [11]. Via the definition of the function $\xi_i(\omega)$ (see equation (7)) or Table 2, it is found that $\xi_1(\omega)$ changes from a negative value to positive as $\omega > \omega_{tT1}$; thus the QC mode in low-frequency range cannot exist in this situation, and it will reduce to the low-frequency IO phonon mode in the GaN/AlN QWRs. The observation shows that the dispersive equations (10), (11) and (30) for QC and IO modes describe the inner self-consistency of phonon modes nature in Q1D wurtzite rectangular QWR structures. This also illustrates the correctness and reasonableness of the present theories of phonon modes. Comparing with the corresponding results of the dispersive spectra for QC and IO modes with those in Q2D GaN/AlN quantum wells, there is no reducing behavior between the QC and IO phonon modes [38].

This reveals that the confined dimensionality can influence greatly the dispersive feature of phonon modes in wurtzite nano-structures [29].

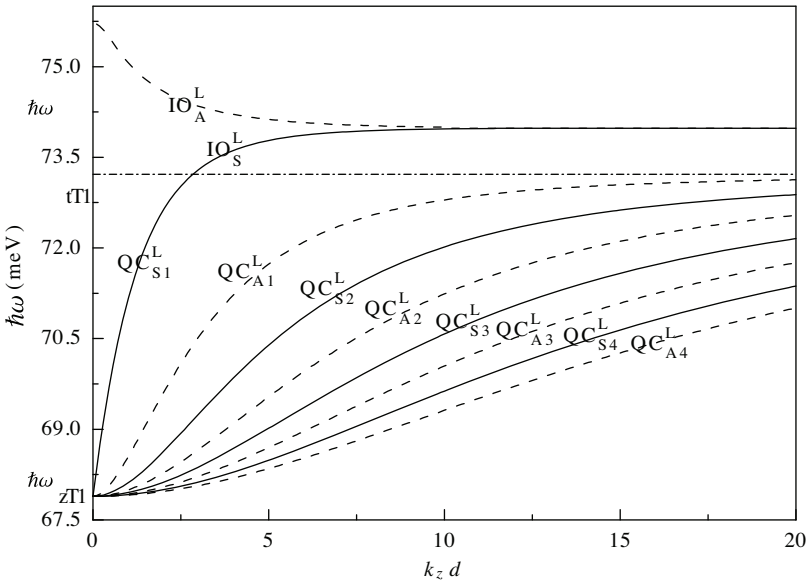

Figure 6. Dispersive spectra of QC modes and IO modes in low-frequency range as a function of k_z in the GaN/AlN QWR system.

At last, we should point out that the DCM and Loudon's uniaxial crystal model [35] are sufficient and valid for the description of phonon modes in the rectangular GaN/AlN QWR with the sizes being $L_x = L_y =$ 5 nm. In general, the efficiency of the DCM is limited to the situation in which the phonon wavelengths are large enough compared with the lattice constant of the semiconductors [56–58]. In fact, the condition that the phonon wavelength (in μm) is far larger than the lattice constant of nitride semiconductors (for GaN, the lattice constant $a = 3.189$ Å and $c = 5.185$ Å [49]) can be easily satisfied. Thus, the DCM can be used to deal with the quantum confined systems with several monolayers (MLs) to tens of MLs [59–61]. Moreover, the experimental results of angular dispersion of polar phonons and Raman scattering, the electron-phonon scattering rates, and the polaronic binding energies in wurtzite heterostructures are proven to be in good agreement with the calculations based on DCM and the Loudon's uniaxial crystal model [13, 30, 58, 6–63]. Hence the numerical results of phonon dispersive spectra on a rectangular QWR with sizes being $L_x = L_y = 5$ nm are valuable and meaningful.

4. Conclusions

In summary, by adopting the DCM and Loudon's uniaxial crystal models, the full polar optical phonon modes including the PR, QC, HS and IO phonon modes in a Q1D wurtzite QWR with rectangular crossing-section have been investigated in the present work. The analytical phonon states and dispersion equations as well as polar polarization eigenvectors for the four types of phonon modes are derived. Each mode has two types of form, i.e. one is symmetrical mode, and the other is antisymmetrical due to the symmetry of the rectangular QWR structures. Numerical calculations are performed on a wurtzite GaN/AlN rectangular

QWR. That three types of phonon mode including the QC, HS and IO modes can appear in the GaN/AlN QWR system is confirmed. The features of dispersive spectra for these modes are displayed and analyzed. The reducing behavior of different types of phonon mode are observed in the Q1D wurtzite rectangular QWR. It is found that the symmetrical QC mode reduces to the symmetrical IO mode as their frequencies approach the characteristic frequency ω_{tL1} of GaN material, which reveals that the present theories of phonon modes are self-consistency and correct for the description of phonon modes in wurtzite Q1D rectangular QWR. This is different obviously from the situation of wurtzite Q2D QWs [38].

These observations show that the confined dimensionality and cross-section shape can influence greatly the dispersive properties of phonon modes in low-dimensional quantum structures [28, 29].

The results obtained in the present paper are quite useful for further investigating the polaronic effect and have significant meaning for analyzing experimental phonon spectra, and for some important optoelectric device designs and applications based on the Q1D GaN-based rectangular QWR structures [26].

Acknowledgments

This work was jointly supported by the National Natural Science Youth Foundation of China (Grant No. 60906042), Yangcheng Scholar Project (Grant No. 10B010D) and Science and Technology Project of Advanced Academy of Guangzhou City (Grant No. 10B001).

References

[1] H. Y. Xu, Z. Liu, Y. Liang, Y. Y. Rao, X. T. Zhang and S. K. Hark, *Appl. Phys. Lett.*, **95**, (2009), 133108.

[2] L. Fu, Z. Chen, D. Wang, L. Cheng, H. Xu, J. Liu, H. Cong, G. Q. Lu and J. Zou, *J. Phys. Chem.,* **C 114**, (2010), 9627.

[3] J. B. Schlager, N. A. Sanford, K. A. Bertness and A. Roshko *J. Appl. Phys.*, **109**, (2011), 044312.

[4] S. Baskoutas A. F. Terzis, *J. Appl. Phys.*, **98**, (2005), 044309.

[5] W. Han, S. Fan, Q. Li and Y. Hu, *Science*, **277**, (1997), 1287.

[6] S. Nakamura S. F. Chichibu, Introduction to Nitride Semiconductor Blue Lasers and Light Emitting Diodes (Taylor and Francis, London, 2000), p.1.

[7] S. C. Jain, M. Willander, J. Narayan and R. V. Overstraeten *J. Appl. Phys.,* **87**, (2000), 965.

[8] W. Lu C.M. Lieber, *J. Phys. D: Appl. Phys.,* **39**, (2006), R387.

[9] L.C. Lew Yan Voon, Y. Zhang, B. Lassen, M. Willatzen, Q. Xiong and P. C. Eklund, *J. Nanosci. Nanotech.,* **8**, (2008), 1.

[10] H. J. Choi, J. C. Johnson, R. He, S. K. Lee, F. Kim, P. Pauzauskie, J. Goldberger, R. J. Saykally and P. Yang, *J. Phys. Chem.,* **B 107**, (2003), 8721.

[11] L. Zhang, J. Shi and T. L. Tansley, *Phys. Rev.,* **B 71**, (2005), 245324.

[12] D. E. N. Brancus, L. Ion, *Phys. Rev.,* **B 76**, (2007), 155304.

[13] L. Zhang, J. J Shi and P. M. Shao, *J. Appl. Phys.,* **110**, (2011), 013712.

[14] J.X. Fang D. Lu, Solid State Physics, book 1, (Shanghai Science and Technology Press, Shanghai 1981), p.192.

[15] N. Telang S. Bandyopadhyay, *Phys. Rev.,* **B 48**, (1993), 18002.

[16] X. Zhang, Z. Liu, C. Wong and S. Hark, *Solid State Commun.,* **139**, (2006), 387.

[17] K. Jeganathan, R. K. Debnath, R. Meijers, T. Stoica, R. Calarco, D. Grutzmacher and H. Luth, *J. Appl. Phys.,* **105**, (2009), 123707.

[18] A. Y. Maslov O. V. Proshina, *Nanoscale Res. Lett.,* **5**, (2010), 1744.

[19] X. F. Duan, Y. Huang, R. Agarwal and C. M. Lieber, *Nature,* **421**, (2003), 241.

[20] T. Yanagishita, M. Sasaki, K. Nishio and H. Masuda, *Adv. Mater.,* **16**, (2004), 429.

[21] D. F. Zhang, L. D. Sun and C. H. Yan, *Chem. Phys. Lett.,* **422**, (2006), 46.

[22] V. P. Solorzano, A. Groning, H. Schweizer and M. Jetter, *Phys. Stat. Sol.,* **B 242**, (2005), R97.

[23] B. Liu, Y. Bando, C. Tang, F. Xu and D. Golberg, *Appl. Phys. Lett.,* **87**, (2005), 073106.

[24] S. Gradecak, F. Qian, Y. Li, H.-G. Park and C. M. Lieber, *Appl. Phys. Lett.,* **87**, (2005), 173111.

[25] T. Kuydendall, P. Pauzauskie, S. Lee, Y. Zhang, J. Goldberger and P. Yang, *Nano Lett.,* **3**, (2003), 1063.

[26] T. Tanaka, K. Uchida, S. Kawanaka and S. Minagawa, *Solid State Electron.,* **41**, (1997), 255.

[27] H. J. Xie, C. Y. Chen and B. K. Ma, *Phys. Rev.* **B 61** (2000), 4827; *J. Phys.: Condens. Matter,* **12**, (2000), 8623.

[28] F. Comas, N. Studart and G. E. Marques, *Solid State Commun.,* **130**, (2004), 477.

[29] K.W. Adu, Q. Xiong, H. R. Gutierrez, G. Chen and P. C. Eklund, *Appl. Phys.,* **A 85**, (2006), 287.

[30] L. Zhang, J. J. Shi and S. Gao, *Semicond. Sci. Tech.,* **23**, (2008), 045014.

[31] M. A. Stroscio, *Phys. Rev.,* **B 40**, (1989), 6428.

[32] M. A. Stroscio, K. W. Kim, M. A. Littlejohn and H. Chuang, *Phys. Rev.,* **B 42**, (1990), 1488.

[33] K. W. Kim, M. A. Stroscio, A. Bhatt, R. Mickevicius and V. V. Mitin, *J. Appl. Phys.,***70**, (1991), 319.

[34] L. Zhang and H. J. Xie, *J. Phys.: Condens. Matter*, **15**, (2003), 5881.

[35] R. Loudon, *Adv. Phys.,* **13**, (1964), 423.

[36] J. J. Shi, *Phys. Rev.,* **B 68**, (2003), 165335.

[37] B. C. Lee, K. W. Kim, M. A. Stroscio and M. Dutta, *Phys. Rev.,* **B 58**, (1998), 4860.

[38] S. M. Komirenko, K. W. Kim, M. A. Stroscio and M. Dutta, *Phys. Rev.,* **B 59**, (1999), 5013.

[39] C. L. Hsiao, L. W. Tu, T. W. Chi, M. Chen, T. F. Young, C. T. Chia and Y. M. Chang, *Appl. Phys. Lett.,* **90**, (2007), 043102.

[40] Y. M. Chang, H. W. Chu, C. H. Shen and S. Gwo, *Appl. Phys. Lett.,* **90**, (2007), 072110.

[41] L. Zhang, *Surf. Rev. Lett.,*, **13**, (2006), 75.

[42] J. J. Shi, X. L. Chu and E. M. Goldys, *Phys. Rev.,* **B 70**, (2004), 115318.

[43] J. J. Shi, X. Q. Zhu, Z. X. Liu, S. H. Pan and X. Y. Li, *Phys. Rev.,* **B 55**, (1997), 4670.

[44] O. Landré, D. Camacho, C. Bougerol, Y. M. Niquet, V. Favre-Nicolin, G. Renaud, H. Renevier and B. Daudin, *Phys. Rev., B*, **81**, (2010), 153306.

[45] D. Camacho Mojica and Yann-Michel Niquet, *Phys. Rev.,* **B**, **81**, (2010), 195313.

[46] L. Rigutti, F. Fortuna, M. Tchernycheva, A. De Luna Bugallo, G. Jacopin, F. H. Julien, S. T. Chou, Y. T. Lin, L. W. Tu and J.-C. Harmand, *Phys. Status Solidi,* **C**, **7**, (2010), 2233.

[47] V. Laneuville, F. Demangeot, R. Pechou, P. Salles, and A. Ponchet, G. Jacopin, L. Rigutti, A. de Luna Bugallo, M. Tchernycheva, and F. H. Julien, K. March and L. F. Zagonel and R. Songmuang, *Phys. Rev.,* **B**, **83**, (2010), 115417.

[48] Julien Renard, Benoit Amstatt, Catherine Bougerol, Edith Bellet-Amalric, Bruno Daudin and Bruno Gayral, *J. Appl. Phys.*, **104**, (2008), 103528.

[49] H. Harima, *J. Phys.: Condens. Matter*, **14**, (2002), R967.

[50] V. Y. Davydov, I. N. Goncharuk, A. N. Smirnov, A.E. Nikolaev, W. V. Lundin, A. S. Usikov, A. A. Klochikhin, J. Aderhold, J. Graul, O. Semchinova and H. Harima, *Phys. Rev.,* **B**, **65**, (2002), 125203.

[51] M. Holtz, T. Prokofyeva, M. Seon, K. Copeland, J. Vanbuskirk, S. Williams, S. A. Nikishin, V. Tretyakov and H. Temkin, *J. Appl. Phys.*, **89**, (2001), 7977.

[52] C. Bungaro and S. de Gironcoli, *Appl. Phys. Lett.*, **76**, (2000), 2101.

[53] Y. G. Cao, X. L. Chen, Y. C. Lan, J.Y. Li, Y. Zhang, Z. Yang and J. K. Linag, *Appl. Phys.,* **A**, **72**, (2001), 125.

[54] E. L. Albuquerque, E. B. Barros, V. N. Freire and J. Mendes-Filho, *Phys. Lett.*, **A**, **336**, (2005), 259.

[55] R. Enderlein, *Phys. Rev.* **B 47**, (1993), 2162.

[56] K. Huang and B. Zhu, *Phys. Rev.*, **B**, **38**, (1988), 13377.

[57] P. A. Knipp and T. L. Reinecke, *Phys. Rev.*, **B**, **46**, (1992), 10310.

[58] H. Rucker, E. Molinari and P. Lugli, *Phys. Rev.*, **B**, **45**, (1992), 6747.

[59] Ph. Lambin, P. Senet and A. A. Lucas, *Phys. Rev.*, **B**, **44**, (1991), 6416.

[60] K. Huang and B. F. Zhu, *Phys. Rev.*, **B**, **38**, (1988), 2183.

[61] S. F. Ren, W. Chen and Y. Y. Peter, *Phys. Rev.*, **B**, **69**, (2004), 235327.

[62] J. Gleize, F. Demangeot, J. Frandon, M. A. Rennci, M. Kuball, B. Daudin and N. Grandjean, *Phys. Stat. Sol.*, **A**, **183**, (2001), 157.

[63] J. Gleize, J. Frandon, F. Demangeot, M. A. Renucci, M. Kuball, J. M. Hayes, F. Widmann and B. Daudin, *Mater. Sci. Eng.*, **B**, **82**, (2001), 27.